Microscopic Structure of the Low-Energy Electric Dipole Response of ^{120}Sn

M. Weinert[1,*] M. Spieker[2], G. Potel[3], N. Tsoneva[4], M. Müscher[1], J. Wilhelmy,[1] and A. Zilges[1]

[1]Institute for Nuclear Physics, University of Cologne, 50937 Köln, Germany
[2]Department of Physics, Florida State University, Tallahassee, Florida 32306, USA
[3]Lawrence Livermore National Laboratory, Livermore, California 94550, USA
[4]Extreme Light Infrastructure (ELI-NP), Horia Hulubei National Institute of Physics and Nuclear Engineering (IFIN-HH),
Bucharest-Măgurele RO-077125, Romania

The microscopic structure of the low-energy electric dipole response, commonly denoted as pygmy dipole resonance (PDR), was studied for ^{120}Sn in a ^{119}Sn$(d, p\gamma)^{120}$Sn experiment. Unprecedented access to the single-particle structure of excited 1^- states below and around the neutron-separation threshold was obtained by comparing experimental data to predictions from a novel theoretical approach. The novel approach combines detailed structure input from energy-density functional plus quasiparticle-phonon model theory with reaction theory to obtain a consistent description of both the structure and reaction aspects of the process. The presented results show that the understanding of one-particle–one-hole structures of the 1^- states in the PDR region is crucial to reliably predict properties of the PDR and its contribution to nucleosynthesis processes.

The first joint detection of gravitational and electromagnetic radiation from a single source, the binary neutron star merger GW170817 [1], provided a new window into heavy-element nucleosynthesis. Triggered by the electromagnetic signals from the optical transient [2,3], neutron star mergers are now again heavily discussed as one of the main sites of the r process [4].

Nuclear physics plays a crucial role in the interpretation of the observables, in particular, of the final isotope abundance patterns. Different nuclear physics inputs like masses, β-decay half-lives, β-delayed neutron emission probabilities, fission properties of heavy nuclei, and neutron-capture rates shape the final abundance pattern [4,5]. Their importance varies depending on the environment where the r-process nucleosynthesis occurs. One possible scenario is the hot r process, where an equilibrium between neutron capture and the inverse photodissociation reactions is generally assumed. Here, the reaction flow would be largely driven by nuclear masses. But even in the hot r process, individual (n, γ) rates can become important at late times, once the $(n, \gamma) \rightleftharpoons (\gamma, n)$ equilibrium is broken [6], and the (n, γ) reactions start to compete against the other processes. To correctly model neutron capture and the inverse photodissociation reactions, it is crucial to understand nuclear structure and the details of the photoresponse near the neutron-separation threshold S_n since both can have a crucial impact in the entrance and decay channels. Especially for the photodissociation reactions, the photoresponse becomes important due to the exponentially decreasing Planck distribution of photons from heated stellar objects. The interaction of photons with atomic nuclei is generally a key ingredient for nucleosynthesis processes, not only for the r process. For example, the high ^{86}Kr/^{82}Kr ratios measured in large star dust SiC grains have been explained by the increase of the ^{85}Kr$(n, \gamma)^{86}$Kr reaction rate for the s-process branching point nucleus ^{85}Kr due to the presence of additional low-energy electric dipole ($E1$) strength around S_n [7].

It has been shown that many nuclei show a concentration of $E1$ strength close to and above S_n, which is usually referred to as the pygmy dipole resonance (PDR) [8,9]. The PDR has attracted a lot of interest during the past two decades, partly due to its possible sensitivity to certain parameters of the nuclear equation of state [10–12], also describing neutron stars [13–18], and its implications for nucleosynthesis processes [6,19–21].

In this Letter, we refer to the PDR as a concentration of excited $J^\pi = 1^-$ states around and below S_n without implying any specific structure such as the macroscopic, dipole-type neutron-skin oscillation often discussed in literature and first introduced in Ref. [22]. We want to stress that in the PDR region states with different isospin character have already been identified by comparing experimental data obtained with hadronic probes at intermediate energies and real-photon scattering [9,23–35]. In heavier nuclei, two distinct groups were observed, suggesting a splitting of the PDR into at least two groups of different isospin character and underlining the presence of different structures [23,25,30].

One of the missing pieces in understanding the structures present in the PDR region is systematic studies of the one-particle–one-hole ($1p$-$1h$) components contributing to

the overall structure of the 1^- states. The neutron $1p$-$1h$ components are of special importance as they have been identified as possible doorway states shared between neutron and γ channels in (n, γ) reactions [36]. As doorway states, the 1^- states of the PDR are expected to strongly influence (n, γ) cross sections and, thus, to impact isotope production in explosive stellar environments. A recent ^{208}Pb(d, p) study showed how neutron $1p$-$1h$ structures could be accessed in the PDR region [37]. A comparison of the experimental observables to theoretical predictions enabled a detailed study of the single-particle character of the 1^- states. Because of its doubly magic character, ^{208}Pb is, however, a special case with a rather small number of 1^- states below the particle-emission threshold making detailed spectroscopy in general more feasible. For most nuclei relevant for the r process, the level density around the threshold could be much higher, calling for a yet missing test of theoretical models.

In this Letter, we report on results from a ^{119}Sn$(d, p\gamma)^{120}$Sn experiment performed at the University of Cologne with the combined SONIC@HORUS setup for coincident particle-γ spectroscopy to study the PDR in an open-shell nucleus with much higher level density. The new experimental approach combines the modest in-beam particle energy resolution of passivated implanted planar silicon (PIPS) detectors and the excellent in-beam γ-ray energy resolution obtained from high-purity germanium (HPGe) detectors with the (d, p) reaction's selectivity to neutron $1p$-$1h$ excitations to study the 1^- states via their $E1$ decays to the ground state. The selection of ground-state decays largely enhances the selectivity to 1^- states and, in general, provides access to PDR states in regions of high level density, i.e., where (d, p) would populate several states with different spins and parity quantum numbers. Thus, $(d, p\gamma)$ with HPGe detectors holds great promise to resolve the PDR states even in nuclei with high level density. In addition, we present a novel theoretical approach combining structure input from energy-density functional (EDF) plus quasiparticle-phonon model (QPM) theory with reaction theory, which consistently integrates the structure into the reaction part for calculating the differential (d, p) cross sections. The same observables as in the $(d, p\gamma)$ experiment are accessed since the γ-decay behavior to the ground state of ^{120}Sn can be accounted for in the QPM on a state-by-state basis. It will be shown that understanding the specific structure of the 1^- states in the PDR region is crucial to correctly model their population in nuclear reactions and their subsequent decay. The observed population of only the lower group of 1^- states questions the applicability of statistical approaches for (n, γ) in the region of the PDR even for nuclei with high level density around the separation threshold.

Setup and experiment.—The experiment was performed at the 10 MV FN Tandem accelerator laboratory of the University of Cologne with a deuteron beam of $E_d = 8.5$ MeV, impinging on a self-supporting and
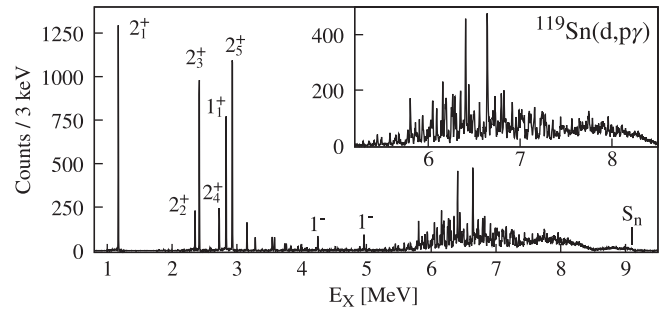

FIG. 1. Ground-state γ-decay spectrum for excited states in ^{120}Sn. Because of selective gates, the spectrum is free of any contaminants. Marked are ground-state decays from several known states in ^{120}Sn and the neutron separation energy S_n. The inset shows the energy region of interest, where the low-energy dipole response is concentrated. Note the clear gap between the discrete transitions at lower energies and the resonancelike structure starting at around 6 MeV possibly corresponding to the gap between the $3\hbar\omega$ and $4\hbar\omega$ harmonic oscillator shells.

enriched ^{119}Sn target (0.39 mg/cm^2, 93.2% enrichment). The SONIC@HORUS setup [38] consisted of four $\Delta E - E$ PIPS telescope detectors mounted under backward angles of $\Theta_p = 122, 131°$ and 14 HPGe detectors surrounding the target chamber. The $\Delta E - E$ detectors were used to identify the (d, p) reaction in the off-line analysis, and the energies of coincidently detected γ rays were corrected for the Doppler shift depending on the angle between the recoiling nucleus and the emitted γ ray. Direct γ decays to the ground state of ^{120}Sn could be investigated by demanding that the excitation energy E_x is equal to the γ-ray energy $E_\gamma \pm 100$ keV. The γ-ray spectrum shown in Fig. 1 was obtained by applying a time-background correction, gating on residual protons, and selecting γ decays to the ground state. The Doppler corrected and gated γ-ray spectrum has been recalibrated using known $J = 1$ states from a recent (γ, γ') measurement [39]. In total, 64 of the 80 discrete lines found in the region above $E_x = 4.5$ MeV correspond to known states with a spin of $J = 1$ and assumed negative parity. We want to stress that, due to the conditions applied to the data, the spectrum is free from any contaminants. Thus, an unambiguous analysis could be performed.

The granularity of the setup allows for the identification of dipole transitions via proton-γ angular correlations. Examples for resolved transitions and continuous distributions can be found in Supplemental Material [40]. For excitation energies below 8 MeV, dipole-type γ-ray ground-state decays do clearly dominate in the PDR region. Above 8 MeV, the angular correlations become more isotropic, possibly indicating either contributions from other multipolarities or a decreasing alignment after the reaction. The $M1$ contribution is negligibly small below 8 MeV as shown in Ref. [41]. Up to 8 MeV, the ground-state γ decays stem predominantly from $J^\pi = 1^-$ states populated in the $(d, p\gamma)$ experiment.
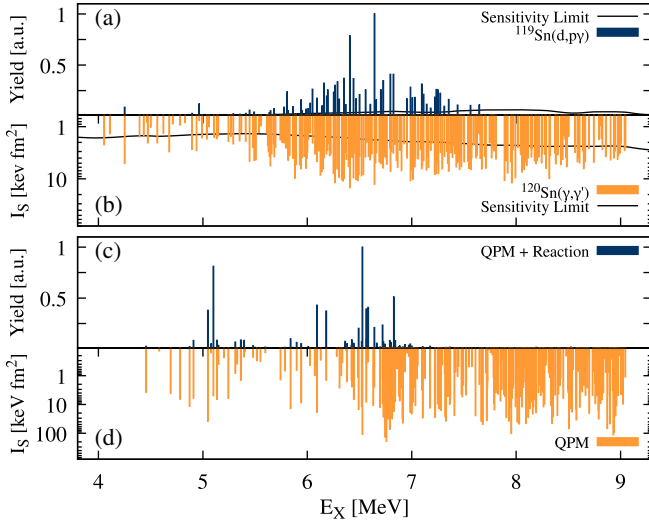
FIG. 2. (a) Relative γ-ray yields from ^{119}Sn$(d, p\gamma)$ and (b) energy-integrated cross sections I_S for ^{120}Sn(γ, γ') adopted from Ref. [39]. All transitions shown in (a) were also observed in the NRF experiment. Sensitivity limits are based on a maximum error on the peak area of 30%. (c) Relative ^{119}Sn$(d, p\gamma)$ yields from the QPM + reaction formalism and (d) predicted energy-integrated cross sections, both taking into account γ-decay branching predicted by the QPM. Theoretical (d, p) cross sections were calculated at scattering angles identical to the experiment. Experimental and theoretical yields were normalized to the strongest transition, respectively. a.u. stands for artificial units.

The experimental relative $(d, p\gamma)$ yields and the energy-integrated nuclear resonance fluorescnence (NRF) cross sections I_S from Ref. [39] are shown in Figs. 2(a) and 2(b). Strikingly, only the lower group of 1^- states with excitation energies $E_x \lesssim 8$ MeV is observed in the $(d, p\gamma)$ reaction with the ground-state γ-decay channel gate applied [see Fig. 2(a)]. The two groups feature states which are equally strongly populated in (γ, γ'), but not in $(d, p\gamma)$. With the $(d, p\gamma)$ sensitivity limit not being the limiting factor [compare Fig. 2(a)], neutron $1p$-$1h$ structure differences might, thus, explain the rather prominent experimental result of only observing the lower group of states in the ground-state γ-decay channel after the (d, p) reaction. To further test this hypothesis, EDF + QPM structure calculations were performed.

Theoretical approach.—In this novel approach, the nuclear excitations are expressed in terms of quasiparticle-random-phase-approximation (QRPA) phonons,

$$Q_{\lambda\mu i}^+ = \frac{1}{2}\sum_{jj'}[\psi_{jj'}^{\lambda i}A_{\lambda\mu}^+(jj') - \varphi_{jj'}^{\lambda i}\tilde{A}_{\lambda\mu}(jj')], \qquad (1)$$

where the set of quantum numbers $j \equiv (nljm\tau)$ labels single-nucleon states, and $A_{\lambda\mu}^+$ and $\tilde{A}_{\lambda\mu}$ are the time-forward and time-backward two-quasiparticle operators, creating or annihilating two quasiparticles coupled to a total angular

momentum λ with projection μ [42]. The excitation energies of the phonons and the time-forward and time-backward amplitudes $\psi_{j_1 j_2}^{\lambda i}$ and $\varphi_{j_1 j_2}^{\lambda i}$ in Eq. (1) are determined by solving QRPA equations [42]. The present QPM calculations follow the model approach and methodology described in Ref. [43]. The wave functions Ψ_ν of the excited QPM 1^- states ν of an even-even nucleus contain contributions from one-, two-, and three-phonon configurations,

$$\Psi_\nu = \left\{ \sum_i R_i(\nu)Q_{1Mi}^+ + \sum_{\substack{\lambda_1 i_1 \\ \lambda_2 i_2}} P_{\lambda_2 i_2}^{\lambda_q i_1}(\nu)[Q_{\lambda_1\mu_1 i_1}^+ \times Q_{\lambda_2\mu_2 i_2}^+]_{1M}\right.$$
$$+ \sum_{\substack{\lambda_1 i_1 \lambda_2 i_2 \\ \lambda_3 i_3 I}} T_{\lambda_3 i_3}^{\lambda_1 i_1 \lambda_2 i_2 I}(\nu)\left[[Q_{\lambda_1\mu_1 i_1}^+ \times Q_{\lambda_2\mu_2 i_2}^+]_{IK}\right.$$
$$\left. \times Q_{\lambda_3\mu_3 i_3}^+\right]_{1M}\left.\right\}\Psi_0, \qquad (2)$$

where the R, P, and T coefficients are the one-, two-, and three-phonon amplitudes, respectively, and Ψ_0 is the ground-state wave function of the even-even nucleus ^{120}Sn (phonon vacuum). The QPM model space includes two- and three-phonon configurations resulting from the coupling of $J^\pi = 1^\pm - 6^\pm$ QRPA phonons up to $E_x = 9$ MeV. For the dipole excitations, one-phonon states up to $E_x = 35$ MeV are taken into account, so that the isovector giant dipole resonance core polarization contributions to the $E1$ transitions of the low-lying 1^- states are taken into account explicitly and without effective charges. Since ground-state correlations are predicted to be small, i.e., the QRPA backward amplitudes are small, the ^{119}Sn target is assumed to be a pure $3s_{1/2}$ hole relative to the ^{120}Sn "core." Experimental data from ^{118}Sn$(t, d)^{119}$Sn support that the ground state of ^{119}Sn is indeed dominated by a hole (particle) in the neutron $3s_{1/2}$ orbital [44,45]. Within this approximation, the ^{119}Sn$(d, p)^{120}$Sn reaction populates QPM 1^- states that contain $3p_{1/2}$ and $3p_{3/2}$ one-quasiparticle states, i.e., states with neutron $(3s_{1/2})^{-1}(3p_{1/2})^{+1}$ and $(3s_{1/2})^{-1}(3p_{3/2})^{+1}$ $1p$-$1h$ components. The corresponding angular differential cross section populating a QPM 1^- state ν in a one-step process results from the coherent contribution of these two components:

$$\frac{d\sigma_\nu}{d\Omega}(\theta) = \frac{\mu_i\mu_f}{(2\pi\hbar^2)^2}\frac{k_f}{k_i} \times |u_{3p_{1/2}}R_{3p_{1/2}}(\nu)\psi_{\frac{1}{2}\frac{1}{2}}^{3p_{1/2}}\mathcal{T}_{p_{1/2}}(\theta)$$
$$+ u_{3p_{3/2}}R_{3p_{3/2}}(\nu)\psi_{\frac{1}{2}\frac{3}{2}}^{3p_{3/2}}\mathcal{T}_{p_{3/2}}(\theta)|^2, \qquad (3)$$

where θ is the deflection angle, μ_i, μ_f are the reduced masses in the incident and outgoing channels, k_i, k_f are the respective momenta, and $u_{3p_{3/2}}$, $u_{3p_{1/2}}$ are the one-quasiparticle occupation numbers obtained by solving BCS

equations [42]. $\mathcal{T}_{p_{1/2}}$ and $\mathcal{T}_{p_{3/2}}$ are the distorted wave Born approximation (d, p) T matrices (see, e.g., Ref. [46]) populating the corresponding $p_{1/2}$ and $p_{3/2}$ states, calculated by using global optical potentials taken from Refs. [47,48]. Note that two-phonon and three-phonon components could only be excited in multistep processes, which are not considered here. No multistep contributions were, however, observed in the $^{207}\text{Pb}(d, p)^{208}\text{Pb}$ experiment [37].

Taking into account the ground-state γ-decay branching, which can be calculated in the QPM on a state-to-state basis [49,50], the theoretical (d, p) cross sections as well as the predicted reduced $B(E1)$ transition strengths can be converted into relative $(d, p\gamma)$ yields and energy-integrated NRF cross sections I_S. The theoretical results for these quantities are presented in Figs. 2(c) and 2(d).

The EDF + QPM approach also allows access to the details of the wave functions. The squared one-phonon amplitudes R^2 are shown in Fig. 3(a). Several $1p$-$1h$ components contribute to the structure of the 1^- states with comparably large amplitudes below an excitation energy of about 7.5 MeV. However, as mentioned earlier, only the $(3s_{1/2})^{-1}(3p_{1/2})^{+1}$ and $(3s_{1/2})^{-1}(3p_{3/2})^{+1}$ components as part of the QRPA 1^- phonons contributing to the QPM states will be populated in $^{119}\text{Sn}(d, p)$. They are highlighted separately in Fig. 3(a) and dominate the one-phonon structure for a number of excited 1^- states. Since ^{120}Sn, in contrast to ^{208}Pb, is an open-neutron-shell nucleus $(N = 70)$, two- and three-phonon configurations already

contribute at lower energies [compare Fig. 3(b)]. Below 7 MeV, one-phonon configurations dominate the picture though. Above 7 MeV, two-phonon and three-phonon contributions begin to contribute significantly to the spectral distribution. The γ-decay branching to the ground state and to the two lowest-lying states is shown in Fig. 3(c).

Discussion.—Besides reproducing the large number of 1^- states observed in the recent (γ, γ') experiment [39], the QPM + reaction formalism correctly predicts that only the lower group of 1^- states is populated in $(d, p\gamma)$ and in the (d, p) reaction in general. Given the high level density and even though the details of the strength fragmentation are different, this in itself is a significant result showing that the EDF + QPM approach does not only correctly predict the approximate location of the relevant single-particle levels around ^{208}Pb but also in the region of the Sn isotopes, while correctly fragmenting the spectroscopic strength to the lower group of states. We, thus, want to stress again that single-particle energies were neither determined from nor adjusted to data. Instead, they were directly obtained at the mean-field level from the EDF [43], maintaining the predictive power of this approach.

The experimental centroid energy determined in the ground-state γ-decay channel, including both $3p_{3/2}$ and $3p_{1/2}$, is 6.49 MeV. The QPM + reaction approach predicts the corresponding centroid energy at 6.32 MeV, in excellent agreement with experiment. The importance of these orbitals for direct-semidirect neutron capture near the $N = 82$ shell closure has been pointed out in Ref. [51].

In addition, very good agreement is obtained for the energy-integrated NRF cross sections for discrete states that are also observed in $(d, p\gamma)$. Experimentally, a summed energy-integrated cross section of $\sum I_S^{\text{NRF}} = 337(21) \text{ keV fm}^2$ is determined from the NRF data. The weakest relative yields still observed in the $(d, p\gamma)$ experiment were on the order of 1%. The QPM predicts a summed energy-integrated cross section of $\sum I_S^{\text{QPM}} = 243 \text{ keV fm}^2$ and $\sum I_S^{\text{QPM}} = 360 \text{ keV fm}^2$ for states with a theoretical relative $(d, p\gamma)$ yield larger than 1% and 0.5%, respectively.

We want to briefly comment on the discrepancy previously observed between $B(E1)$ strengths determined in NRF [39,52] and two (p, p') experiments performed near $0°$ and at 300 MeV [41,53], which was most pronounced above 6.5 MeV. It was speculated that one possible source contributing to this discrepancy could be γ-decay branching not observed in NRF [39]. As seen in Figs. 3(b) and 3(c), the γ-decay behavior of the 1^- states does indeed change as the states' structure becomes more complex with the average ground-state branching ratio decreasing and the average ratios to excited states increasing. This underlines the need for comparing experimental data and theoretical calculations on the same footing as done in this Letter by limiting the comparison to configurations selectively populated in (d, p), ground-state γ decays, and comparing the
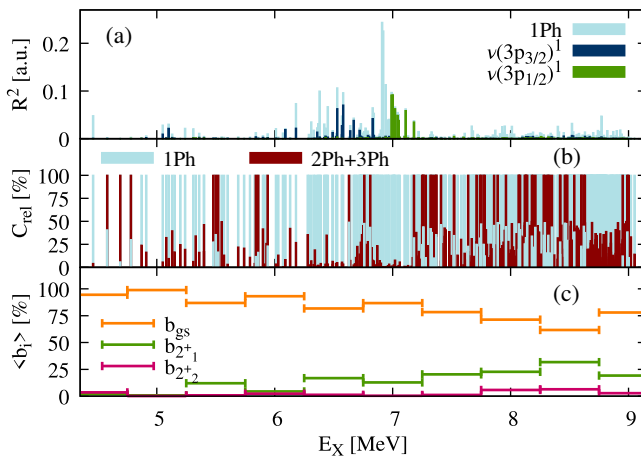

FIG. 3. (a) Summed squared one-phonon R amplitudes for each QPM state, representing the contribution of a given configuration to the final wave function. Individual contributions of neutron $1p$-$1h$ configurations accessible in $^{119}\text{Sn}(d, p)$ are shown in dark blue and green, respectively. Distributions of all configurations can be found in Supplemental Material [40]. (b) Relative 1Ph and 2Ph + 3Ph contributions $C_{\text{rel}}^{1\text{Ph}} = \sum R^2 / \sum(R^2 + P^2 + T^2)$ and $C_{\text{rel}}^{2\text{Ph}+3\text{Ph}} = \sum(P^2 + T^2) / \sum(R^2 + P^2 + T^2)$ to the QPM wave function, as given in Eq. (2). (c) γ-decay branching to the ground state and to the two lowest-lying excited 2^+ states in ^{120}Sn, averaged over all states in a window of 500 keV. a.u. stands for artificial units.

true experimental NRF observable to the consistently calculated QPM quantity. The selective population of only the lower group of states in $(d, p\gamma)$ shows the importance of a consistent description of structure and reaction theory, and the need to thoroughly test the PDR wave functions.

Conclusion.—The PDR has been studied in a ^{119}Sn$(d, p\gamma)^{120}$Sn coincidence experiment. Employing the capabilities of the SONIC@HORUS setup, the reaction channel could be unambiguously selected, eliminating any contaminations in the γ-ray spectra. The excellent energy resolution of the HPGe detectors and the consecutive Doppler correction allowed for the detailed study of the $(d, p\gamma)$ strength distribution for excited $J^\pi = 1^-$ states in the ground-state γ-decay channel. By combining EDF + QPM with reaction theory, the same degree of fragmentation of the spectroscopic strength resulting from the $(3s_{1/2})^{-1}(3p_{1/2})^{+1}$ and $(3s_{1/2})^{-1}(3p_{3/2})^{+1}$ $1p$-$1h$ components could be observed. In addition to the ^{208}Pb region, the EDF + QPM approach does, thus, also reproduce the position of the relevant single-particle levels in the Sn region. The centroid energies were found in excellent agreement. The $l = 1$ orbitals are expected to dominate direct-semidirect neutron capture cross sections around $N = 82$ at low neutron energies [51]. The energy-integrated NRF cross sections were also found in very good agreement for states with these two specific structures, supporting the accuracy of the QPM wave functions. Careful analysis of the QPM results revealed that the currently debated structural change throughout the PDR region, partly causing the discrepancy between (p, p') and (γ, γ') experiments, is indeed predicted by the QPM. Most significantly, the observed splitting of the spectroscopic strength into two groups is intriguing as it closely resembles the isospin splitting observed in ^{124}Sn [29,54]. The neutron $1p$-$1h$ character of the observed states may have significant impact on the prediction of direct-semidirect neutron capture rates [51], especially if the splitting can be observed in even more neutron-rich nuclei. The presented results question the applicability of statistical approaches for the PDR in (n, γ) reactions, since they show that, at least in the PDR region, not the entire γ-ray strength function might play a role as a group of 1^- states is not populated. Employing $(d, p\gamma)$ and the QPM + reaction method for more nuclei and in different mass regions will allow thorough testing of the EDF + QPM calculations on a microscopic level and extend the predictive power for modeling neutron capture in unstable neutron-rich nuclei [51]. The present work underlines that structure plays a significant role for the low-energy $E1$ strength in neutron-rich nuclei not only for generating enhanced $B(E1)$ strengths but also in populating the states in nuclear reactions.

[*] mweinert@ikp.uni-koeln.de

[1] B. P. Abbott, R. Abbott, T. D. Abbott, F. Acernese, K. Ackley *et al.*, Multi-messenger observations of a binary neutron star merger, Astrophys. J. **848**, L12 (2017).

[2] M. R. Drout *et al.*, Light curves of the neutron star merger GW170817/SSS17A: Implications for r-process nucleosynthesis, Science **358**, 1570 (2017).

[3] E. Pian, P. D'Avanzo, S. Benetti, M. Branchesi, E. Brocato *et al.*, Spectroscopic identification of r-process nucleosynthesis in a double neutron-star merger, Nature (London) **551**, 67 (2017).

[4] J. J. Cowan, C. Sneden, J. E. Lawler, A. Aprahamian, M. Wiescher, K. Langanke, G. Martinez-Pinedo, and F. K. Thielemann, Origin of the heaviest elements: The rapid neutron-capture process, Rev. Mod. Phys. **93**, 015002 (2021).

[5] M. Mumpower, R. Surman, G. McLaughlin, and A. Aprahamian, The impact of individual nuclear properties on r-process nucleosynthesis, Prog. Part. Nucl. Phys. **86**, 86 (2016).

[6] A. Larsen, A. Spyrou, S. Liddick, and M. Guttormsen, Novel techniques for constraining neutron-capture rates relevant for r-process heavy-element nucleosynthesis, Prog. Part. Nucl. Phys. **107**, 69 (2019).

[7] R. Raut, A. P. Tonchev, G. Rusev, W. Tornow, C. Iliadis, M. Lugaro, J. Buntain, S. Goriely, J. H. Kelley, R. Schwengner, A. Banu, and N. Tsoneva, Cross-Section Measurements of the ^{86}Kr(γ, n) Reaction to Probe the s-Process Branching at ^{85}Kr, Phys. Rev. Lett. **111**, 112501 (2013).

[8] D. Savran, T. Aumann, and A. Zilges, Experimental studies of the pygmy dipole resonance, Prog. Part. Nucl. Phys. **70**, 210 (2013).

[9] A. Bracco, E. Lanza, and A. Tamii, Isoscalar and isovector dipole excitations: Nuclear properties from low-lying states and from the isovector giant dipole resonance, Prog. Part. Nucl. Phys. **106**, 360 (2019).

[10] J. Piekarewicz, Pygmy dipole resonance as a constraint on the neutron skin of heavy nuclei, Phys. Rev. C **73**, 044325 (2006).

[11] J. Piekarewicz, Pygmy resonances and neutron skins, Phys. Rev. C **83**, 034319 (2011).

[12] X. Roca-Maza and N. Paar, Nuclear equation of state from ground and collective excited state properties of nuclei, Prog. Part. Nucl. Phys. **101**, 96 (2018).

[13] C. J. Horowitz and J. Piekarewicz, Neutron Star Structure and the Neutron Radius of ^{208}Pb, Phys. Rev. Lett. **86**, 5647 (2001).

[14] C. J. Horowitz and J. Piekarewicz, Neutron radii of ^{208}Pb and neutron stars, Phys. Rev. C **64**, 062802(R) (2001).

[15] F. J. Fattoyev and J. Piekarewicz, Neutron skins and neutron stars, Phys. Rev. C **86**, 015802 (2012).

[16] F. J. Fattoyev and J. Piekarewicz, Has a Thick Neutron Skin in ^{208}Pb Been Ruled Out?, Phys. Rev. Lett. **111**, 162501 (2013).

[17] F. J. Fattoyev, J. Piekarewicz, and C. J. Horowitz, Neutron Skins and Neutron Stars in the Multimessenger Era, Phys. Rev. Lett. **120**, 172702 (2018).

[18] M. Thiel, C. Sfienti, J. Piekarewicz, C. J. Horowitz, and M. Vanderhaeghen, Neutron skins of atomic nuclei: Per aspera ad astra, J. Phys. G **46**, 093003 (2019).

[19] S. Goriely, Radiative neutron captures by neutron-rich nuclei and the r-process nucleosynthesis, Phys. Lett. B **436**, 10 (1998).

[20] E. Litvinova, H. Loens, K. Langanke, G. Martínez-Pinedo, T. Rauscher, P. Ring, F.-K. Thielemann, and V. Tselyaev, Low-lying dipole response in the relativistic quasiparticle time blocking approximation and its influence on neutron capture cross sections, Nucl. Phys. **A823**, 26 (2009).

[21] A. Tonchev, N. Tsoneva, C. Bhatia, C. Arnold, S. Goriely, S. Hammond, J. Kelley, E. Kwan, H. Lenske, J. Piekarewicz, R. Raut, G. Rusev, T. Shizuma, and W. Tornow, Pygmy and core polarization dipole modes in ^{206}Pb: Connecting nuclear structure to stellar nucleosynthesis, Phys. Lett. B **773**, 20 (2017).

[22] R. Mohan, M. Danos, and L. C. Biedenharn, Three-fluid hydrodynamical model of nuclei, Phys. Rev. C **3**, 1740 (1971).

[23] D. Savran, M. Babilon, A. M. van den Berg, M. N. Harakeh, J. Hasper, A. Matic, H. J. Wörtche, and A. Zilges, Nature of the Pygmy Dipole Resonance in ^{140}Ce Studied in $(\alpha, \alpha'\gamma)$ Experiments, Phys. Rev. Lett. **97**, 172502 (2006).

[24] J. Endres, D. Savran, A. M. van den Berg, P. Dendooven, M. Fritzsche, M. N. Harakeh, J. Hasper, H. J. Wörtche, and A. Zilges, Splitting of the pygmy dipole resonance in ^{138}Ba and ^{140}Ce observed in the $(\alpha, \alpha'\gamma)$ reaction, Phys. Rev. C **80**, 034302 (2009).

[25] J. Endres, E. Litvinova, D. Savran, P. A. Butler, M. N. Harakeh, S. Harissopulos, R.-D. Herzberg, R. Krücken, A. Lagoyannis, N. Pietralla, V. Y. Ponomarev, L. Popescu, P. Ring, M. Scheck, K. Sonnabend, V. I. Stoica, H. J. Wörtche, and A. Zilges, Isospin Character of the Pygmy Dipole Resonance in ^{124}Sn, Phys. Rev. Lett. **105**, 212503 (2010).

[26] V. Derya, J. Endres, M. Elvers, M. Harakeh, N. Pietralla, C. Romig, D. Savran, M. Scheck, F. Siebenhühner, V. Stoica, H. Wörtche, and A. Zilges, Study of the pygmy dipole resonance in ^{94}Mo using the $(\alpha, \alpha'\gamma)$ coincidence technique, Nucl. Phys. **A906**, 94 (2013).

[27] V. Derya, D. Savran, J. Endres, M. Harakeh, H. Hergert, J. Kelley, P. Papakonstantinou, N. Pietralla, V. Ponomarev, R. Roth, G. Rusev, A. Tonchev, W. Tornow, H. Wörtche, and

A. Zilges, Isospin properties of electric dipole excitations in ^{48}Ca, Phys. Lett. B **730**, 288 (2014).

[28] F. C. L. Crespi *et al.*, Isospin Character of Low-Lying Pygmy Dipole States in ^{208}Pb via Inelastic Scattering of ^{17}O ions, Phys. Rev. Lett. **113**, 012501 (2014).

[29] L. Pellegri *et al.*, Pygmy dipole resonance in ^{124}Sn populated by inelastic scattering of ^{17}O, Phys. Lett. B **738**, 519 (2014).

[30] E. G. Lanza, A. Vitturi, E. Litvinova, and D. Savran, Dipole excitations via isoscalar probes: The splitting of the pygmy dipole resonance in ^{124}Sn, Phys. Rev. C **89**, 041601(R) (2014).

[31] F. C. L. Crespi *et al.*, 1^- and 2^+ discrete states in ^{90}Zr populated via the $(^{17}O^{17}O'\gamma)$ reaction, Phys. Rev. C **91**, 024323 (2015).

[32] M. Krzysiek *et al.*, Pygmy dipole resonance in ^{140}Ce via inelastic scattering of ^{17}O, Phys. Rev. C **93**, 044330 (2016).

[33] N. Nakatsuka *et al.*, Observation of isoscalar and isovector dipole excitations in neutron-rich ^{20}O, Phys. Lett. B **768**, 387 (2017).

[34] F. Crespi *et al.*, Gamma decay of pygmy states in ^{90,94}Zr from inelastic scattering of light ions, J. Phys. Conf. Ser. **1014**, 012002 (2018).

[35] D. Savran, V. Derya, S. Bagchi, J. Endres, M. Harakeh, J. Isaak, N. Kalantar-Nayestanaki, E. Lanza, B. Löher, A. Najafi, S. Pascu, S. Pickstone, N. Pietralla, V. Ponomarev, C. Rigollet, C. Romig, M. Spieker, A. Vitturi, and A. Zilges, Multi-messenger investigation of the pygmy dipole resonance in ^{140}Ce, Phys. Lett. B **786**, 16 (2018).

[36] A. M. Lane, Partial width correlations and common doorway states, Ann. Phys. (N.Y.) **63**, 171 (1971).

[37] M. Spieker, A. Heusler, B. A. Brown, T. Faestermann, R. Hertenberger, G. Potel, M. Scheck, N. Tsoneva, M. Weinert, H.-F. Wirth, and A. Zilges, Accessing the Single-Particle Structure of the Pygmy Dipole Resonance in ^{208}Pb, Phys. Rev. Lett. **125**, 102503 (2020).

[38] S. G. Pickstone, M. Weinert, M. Färber, F. Heim, E. Hoemann, J. Mayer, M. Müscher, S. Prill, P. Scholz, M. Spieker, V. Vielmetter, J. Wilhelmy, and A. Zilges, Combining γ-ray and particle spectroscopy with SONIC@HORUS, Nucl. Instrum. Methods Phys. Res., Sect. A **875**, 104 (2017).

[39] M. Müscher, J. Wilhelmy, R. Massarczyk, R. Schwengner, M. Grieger, J. Isaak, A. R. Junghans, T. Kögler, F. Ludwig, D. Savran, D. Symochko, M. P. Takács, M. Tamkas, A. Wagner, and A. Zilges, High-sensitivity investigation of low-lying dipole strengths in ^{120}Sn, Phys. Rev. C **102**, 014317 (2020).

[40] See Supplemental Material at http://link.aps.org/supplemental/10.1103/PhysRevLett.127.242501 for additional information on the proton-γ angular correlations and a detailed distribution of the one-phonon components from the EDF + QPM calculations.

[41] S. Bassauer *et al.*, Electric and magnetic dipole strength in ^{112,114,116,118,120,124}Sn, Phys. Rev. C **102**, 034327 (2020).

[42] V. G. Soloviev, *Theory of Complex Nuclei* (Pergamon Press, Oxford, 1976).

[43] N. Tsoneva and H. Lenske, Energy–density functional plus quasiparticle–phonon model theory as a powerful tool for

nuclear structure and astrophysics, Phys. At. Nucl. **79,** 885 (2016).

[44] E. Schneid, A. Prakash, and B. Cohen, (d, p) and (d, t) reactions on the isotopes of tin, Phys. Rev. **156,** 1316 (1967).

[45] R. Chapman, M. Hyland, J. L. Durell, J. N. Mo, M. Macphail, H. Sharma, and N. H. Merrill, Neutron orbit sizes in the isotopes of tin, Nucl. Phys. **A316,** 40 (1979).

[46] I. J. Thompson and F. M. Nunes, *Nuclear Reactions for Astrophysics* (Cambridge University Press, Cambridge, England, 2009).

[47] A. J. Koning and J. P. Delaroche, Local and global nucleon optical modes from 1 keV to 200 MeV, Nucl. Phys. **A713,** 231 (2003).

[48] Y. Han, Y. Shi, and Q. Shen, Deuteron global optical model potential for energies up to 200 MeV, Phys. Rev. C **74,** 044615 (2006).

[49] M. Spieker, N. Tsoneva, V. Derya, J. Endres, D. Savran, M. Harakeh, S. Harissopulos, R.-D. Herzberg, A. Lagoyannis, H. Lenske, N. Pietralla, L. Popescu, M. Scheck, F. Schlüter, K. Sonnabend, V. Stoica, H. Wörtche, and A. Zilges, The

pygmy quadrupole resonance and neutron-skin modes in ^{124}Sn, Phys. Lett. B **752,** 102 (2016).

[50] B. Löher *et al.*, The decay pattern of the pygmy dipole resonance of ^{140}Ce, Phys. Lett. B **756,** 72 (2016).

[51] B. Manning *et al.*, Informing direct neutron capture on tin isotopes near the $N = 82$ shell closure, Phys. Rev. C **99,** 041302(R) (2019).

[52] B. Özel-Tashenov, J. Enders, H. Lenske, A. M. Krumbholz, E. Litvinova, P. von Neumann-Cosel, I. Poltoratska, A. Richter, G. Rusev, D. Savran, and N. Tsoneva, Low-energy dipole strength in ^{112,120}Sn, Phys. Rev. C **90,** 024304 (2014).

[53] A. Krumbholz *et al.*, Low-energy electric dipole response in ^{120}Sn, Phys. Lett. B **744,** 7 (2015).

[54] J. Endres, E. Litvinova, D. Savran, P. A. Butler, M. N. Harakeh, S. Harissopulos, R. D. Herzberg, R. Krücken, A. Lagoyannis, N. Pietralla, V. Y. Ponomarev, L. Popescu, P. Ring, M. Scheck, K. Sonnabend, V. I. Stoica, H. J. Wörtche, and A. Zilges, Isospin Character of the Pygmy Dipole Resonance in ^{124}Sn, Phys. Rev. Lett. **105,** 212503 (2010).